ASME TURBO EXPO 2005
June 6-9, 2005, Reno, Nevada
GT2005-69133

Effects of Surface Roughness on Turbine Vane Heat Transfer

R. J. Boyle
NASA Glenn Research Center
Cleveland, Ohio
Robert.J.Boyle@grc.nasa.gov

R. G. Senyitko
QSS Group, Inc.
Cleveland, Ohio
Richard.G.Senyitko@grc.nasa.gov

ABSTRACT

Turbine vane surface temperatures were measured in a linear cascade using an infrared non-contact thermal detector. A thermal barrier coating (TBC) was applied to the vane surface to give a rough surface. The temperature drop across the relatively thick TBC was used to determine heat transfer coefficients. Tests were conducted over a range of Reynolds and Mach numbers, resulting in large variations in hydraulic roughness. The measured heat transfer rates were significantly higher than were expected for a smooth vane. The detector was mounted in a probe holder, and traversed in a manner similar to that used for pneumatic or hot wire probes. The results showed that this approach gave useful information, and should be considered when non-contact surface temperatures are desired.

Nomenclature

C	-	True chord
C_p	-	Pressure coefficient, $(P_{T-1} - P)/(P_{T-1} - P_2)$
C_X	-	Axial chord
h	-	Heat transfer coefficient
k	-	Thermal conductivity
k_S	-	Equivalent roughness height
M	-	Mach number
Nu	-	Nusselt number, hC_X/k_G
q	-	Heat flux
Pr	-	Prandtl number
R_a	-	Roughness measure
Re	-	Reynolds number, $\rho_2 V_2 C_X/\mu_2$
s	-	Surface distance
t_{TBC}	-	TBC thickness
Tu	-	Turbulence intensity,%
V	-	Velocity
x	-	Axial distance
ϵ_S	-	Surface emissivity
μ	-	Molecular viscosity
ρ	-	Density
σ	-	Stefan-Boltzmann constant

Subscripts

AMB	-	Ambient
APP	-	Apparent
CONV	-	Convection
CORR	-	Corrected
CU	-	Copper vane
G	-	Gas total
R	-	Recovery
RAD	-	Radiation
S	-	Surface
TBC	-	Thermal barrier coating
T	-	Total
1	-	Vane row inlet
2	-	Vane row exit

INTRODUCTION

As turbine inlet temperatures increase, the necessity for accurate heat transfer predictions also increases. If Reynolds number and roughness height are sufficiently large, blade heat transfer increases above that for a smooth blade. Accurate predictions of rough surface heat transfer are needed, because increased external heat transfer results in higher blade temperatures, especially if the roughness is due to erosion. Even if the roughness is due to deposition, blade temperatures can increase, since, the added insulation of the deposition can be more than offset by the increased rough surface heat transfer.

Experimental data for rough surface heat transfer have been obtained using both deterministic and random roughness geometry. Deterministic roughness geometry, used by Stripf et al.[1], Barlow et al.[2], Hosni et al.[3], and by Bogard et al.[4], among others, has the advantage of precisely known surface roughness profile. Random roughness as used by Blair[5], Bons[6], Bons and McClain[7], Boyle et al.[8], Abuaf et al.[9], and by Bunker[10], among others, only allows for a statistical representation of the surface roughness. Both types of roughness require that the roughness geometry be transformed into an equivalent

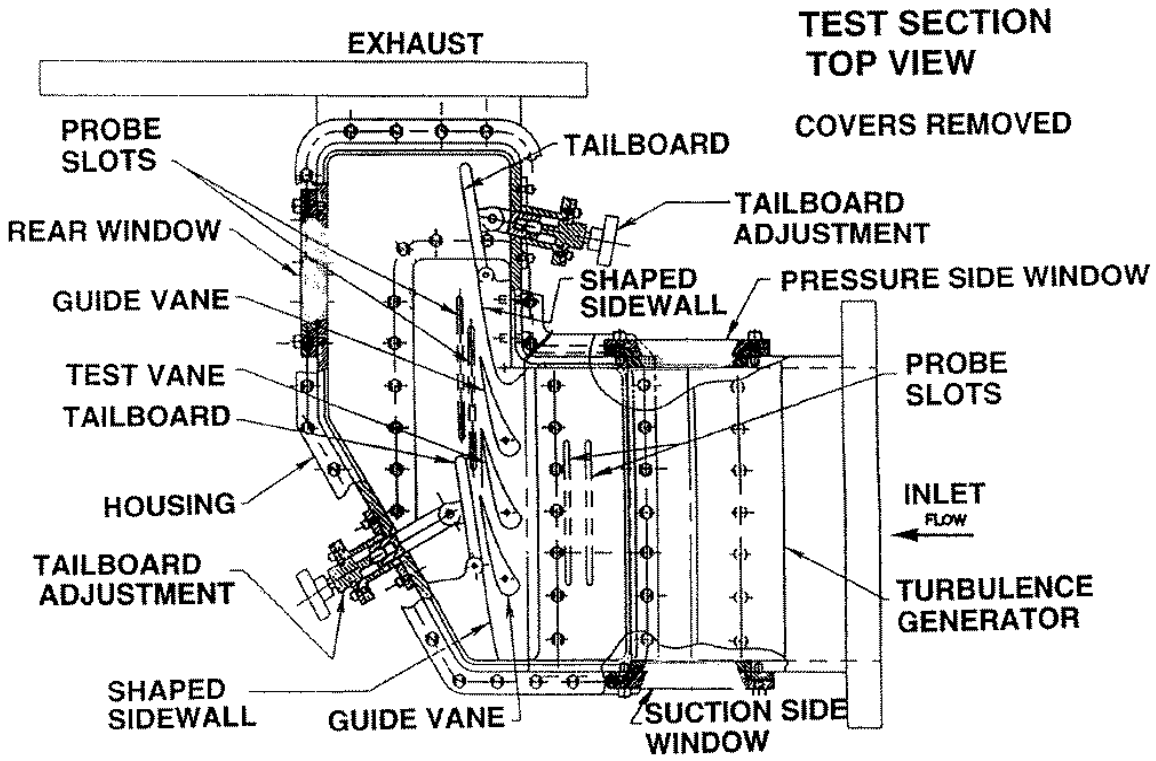

Fig. 1 Overall view of test section.

sand grain roughness, k_S, for use in predictive tools.

Turbine blade surface roughness is due to either erosion or deposition. Measurements for in service vanes and blades by Tarada and Suzuki[11], Taylor[12], and Bons et al.[13] show large variations in surface roughness. The issue of how to convert measured surface roughness into equivalent sand grain roughness has been addressed by several authors. The simplest approach is that of Koch and Smith[14], who give k_S as a multiple of the center line average roughness, R_a. Since very closely spaced roughness approximates a surface displaced by the height of the roughness, it appears to be hydraulically smooth. Widely spaced roughness elements can lose their effectiveness. To account for this behavior, several correlations have been proposed to determine k_S from roughness measurements. Bons[6] proposed a correlation for the roughness height based on the angle of the roughness trace. Sigal and Danberg[15], Dvorak[16], Dirling[17], Waigh and Kind[18], and van Rij et al.[19] have proposed correlations for determining k_S from roughness measurements. In addition, van Rij et al.[19] outlined a method for determining k_S for surfaces with random roughness. Stripf et al.[1] used the correlation of Waigh and Kind[18] to calculate k_S for deterministic roughness of truncated cones of several heights. They also measured heat transfer for cones of the same height with different spacing between cones. Their results showed less sensitivity to spacing than was predicted using the Waigh and Kind[18] correlation. For a given roughness there is a significant variation in k_S among the various correlations.

Even if k_S were known precisely, it is necessary to match Reynolds numbers in order to predict the effects of surface roughness in an engine environment. For this reason the experiments reported herein were done using a single roughness, and a wide range of flow Reynolds numbers in order to obtain a wide range of $Re(k_S)$. In these experiments the roughness parameters are fixed, and k_S is constant, even though it may not be precisely known.

Increasing freestream turbulence shows the same effects on blade heat transfer as does increasing surface roughness. Many investigators measured rough surface heat transfer with high freestream turbulence levels in order to better simulate actual engine operating conditions. However, the tests reported herein were done with an inlet turbulence level close to 1%. This low level was chosen in order to better isolate the effects of surface roughness.

It is necessary to measure the surface temperatures of a rough surface without disturbing the surface. Even thin film thermocouples will distort the surface in the region where they are applied. Hoffs et al.[20] used uniformly applied liquid crystals to give a uniform roughness. But, liquid crystals are often used for smooth blade heat transfer measurements, and may not be sufficiently rough at low Reynolds numbers. Infrared measurements were chosen to measure surface temperatures. Different aspects of film cooling have been studied using infrared cameras, by, among others, Sargent et al.[21], Baldauf et al.[22], Johnston et al.[23], and Sweeney and Rhodes[24]. Boyle et al.[8] used a camera positioned externally to the cascade. However, the camera's view of the test blade was partially

Table I. Vane Characteristics

Axial Chord, C	5.18 cm
True Chord	10.40 cm
Pitch	8.26 cm
Span	21.59 cm
Trailing edge thickness	0.26 cm
Flow turning angle	75°

Table II. Operating range of test conditions

M_2	P_{t-1} (atm)	INLET $Re(C_X)$ $\times 10^{-6}$	EXIT $Re(C_X)$ $\times 10^{-6}$
0.3	0.34	0.030	0.117
	1.36	0.121	0.466
0.9	0.34	0.060	0.255
	1.36	0.239	1.021

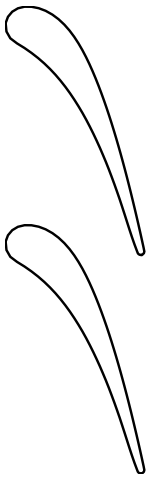

Fig. 2, Test vane and passage.

obscured by adjacent blades. To overcome this limitation an infrared detector was mounted in a probe. The probe was traversed and rotated so as to view a heated blade from several locations. Although the probe was mounted out of the measurement plane, it was still in the flow field. Therefore, a small diameter detector was used, and its output was just a single temperature reading.

The work reported herein discusses surface heat transfer measurements for a single rough surface vane at axial chord exit Reynolds numbers between 0.12 and 1.0×10^6. Vane exit Mach numbers were 0.3 and 0.9. Issues associated with the use of an infrared temperature sensor are also discussed in order to demonstrate the validity of the measurements. Comparisons are also made with two-dimensional CFD heat transfer predictions.

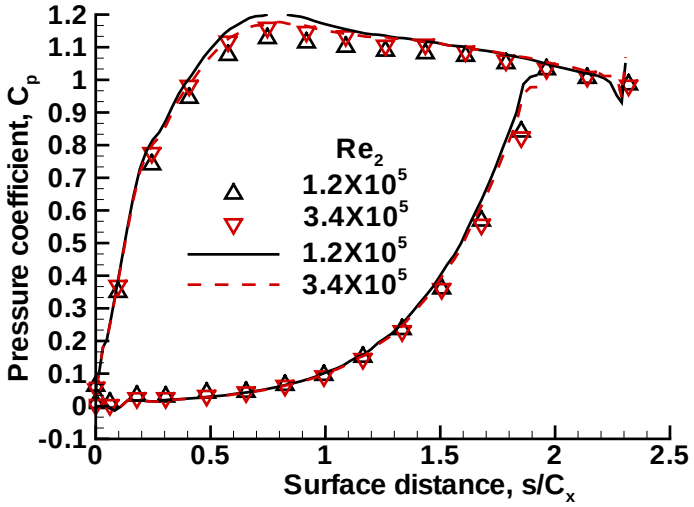

Fig. 3a Predicted and measured pressure coefficients, M_2=0.3

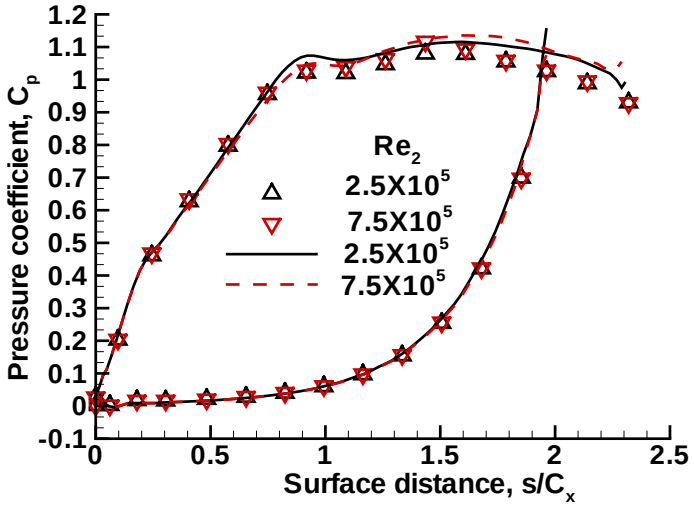

Fig. 3b Predicted and measured pressure coefficients, M_2=0.9

DESCRIPTION of EXPERIMENT

Figure 1 gives an overall view of the cascade. The linear cascade has three vanes and four passages. Adjustable tailboards are used to achieve periodicity for the two passages adjacent to the middle test vane. The original tests for the cascade had pressure instrumentation on all three vanes. These measurements were used to determine the tailboard settings. In the current tests, only the outer two vanes were instrumented with pressure taps. The cascade true chord aspect ratio is 2.08. This high aspect ratio was chosen to achieve two-dimensional flow in the mid-span region, where the heat transfer measurements were made. The cascade was supplied using pressurized air, and the air exited into a low pressure altitude exhaust system. By controlling inlet and exhaust valves, cascade Reynolds and Mach numbers were varied independently. Tests were done

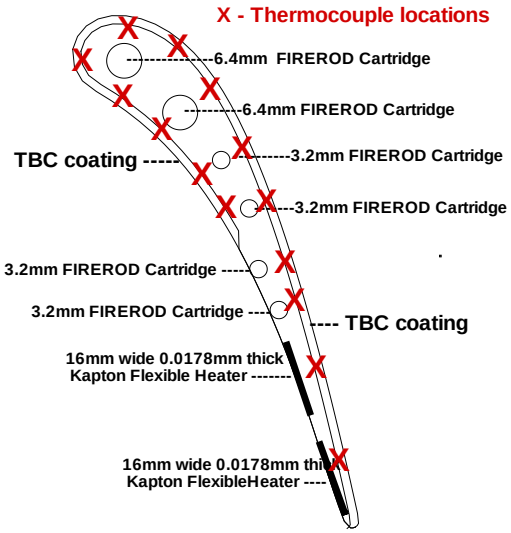

Fig. 4 Heater and thermocouple locations for suction surface test vane.

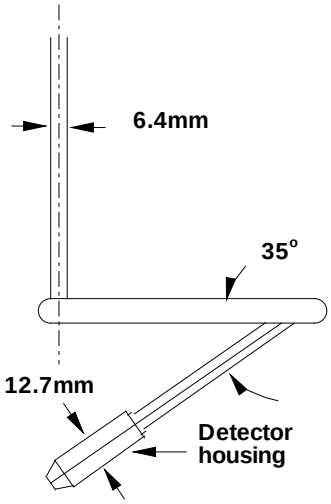

Fig. 5 Infrared detector probe.

with inlet total pressures between 0.3 and 1.3 atms., and vane exit Mach numbers of 0.3 and 0.9. Consequently, the test Reynolds number varied by close to a factor of ten, Further details of the cascade are given by Boyle and Senyitko[25], and by Boyle et al.[8].

Vane characteristics are given in Table I. The vane coordinates were given both by Boyle and Senyitko[25], and by Schwab[26]. Figure 2 shows the test vane and adjacent vane. The incoming flow was axial, and was turned approximately 75 degrees. Table II gives the range of test conditions. The Reynolds number varied by nearly a factor of nine. $Re(C)$ is approximately double $Re(C_X)$.

Figures 3a and 3b show the vane C_p distributions as a function of surface distance. The two Reynolds numbers distributions at each exit Mach number show that the Reynolds number effects are small. Overall, the loadings are conservative. The peak suction surface C_p is only 1.2 at the $M_2 = 0.3$, and is only about 1.1 at $M_2 = 0.9$. While the C_p distributions are similar, there is more diffusion at the lower Mach number. At $M_2 = 0.3$ the suction surface is expected to transition from laminar to turbulent at a lower Reynolds number. These data are for the smooth vane. The predictions were done using the code RVCQ3D run as a two-dimensional Navier-Stokes analysis. Calculations for the effects of surface roughness on pressure distribution showed no noticeable effect of roughness on the pressure distributions. The code RVCQ3D has been documented by Chima.[27], and Chima et al.[28]. Predictions of rough surface heat transfer were also made using this code.

The heat transfer tests were done using a heated copper vane. Figure 4 shows the vane instrumented to measure suction surface heat transfer. The copper vane was undercut by 1.5mm, and a TBC coating was plasma sprayed onto the copper. The conductivity of the TBC was measured and found to be 0.808 W/m/K at 0C, and 0.860 W/m/K at 100C. The measured deviation was ±0.03 W/m/K. The local heat flux was determined by measuring the temperature of the copper and the surface temperature of the TBC. The copper vane was heated using a combination of rod and surface heaters. Two test vanes were used. One had the TBC coating applied to the entire suction surface and the front portion of the pressure surface. Figure 4 shows that this vane had two surface heaters applied to the rear of the pressure surface. Surface, rather than rod, heaters were used on the rear of the vane because downstream of the suction surface throat location the vane is relatively thin. Also shown are the locations of thermocouples used to insure that the copper inner vane was at a near uniform temperature. The copper vane extended over the middle half of the span. Stainless steel end caps, shaped to the outer vane profile, partially insulated the heated vane section from the aluminum test chamber. The end caps were also used to insure a uniform TBC thickness. Measurements using an infrared camera showed very good temperature uniformity in the spanwise direction for over two-thirds of the heated span. Tests were run using various copper temperatures, but the data reported were obtained using a copper temperature near 100C. While TBC coatings are used in engines at much higher temperatures, the coating thickness is less than the 1.5mm thickness used in these tests. The vane used to measure pressure surface heat transfer was similarly constructed, except that the surface heaters were applied to the suction surface.

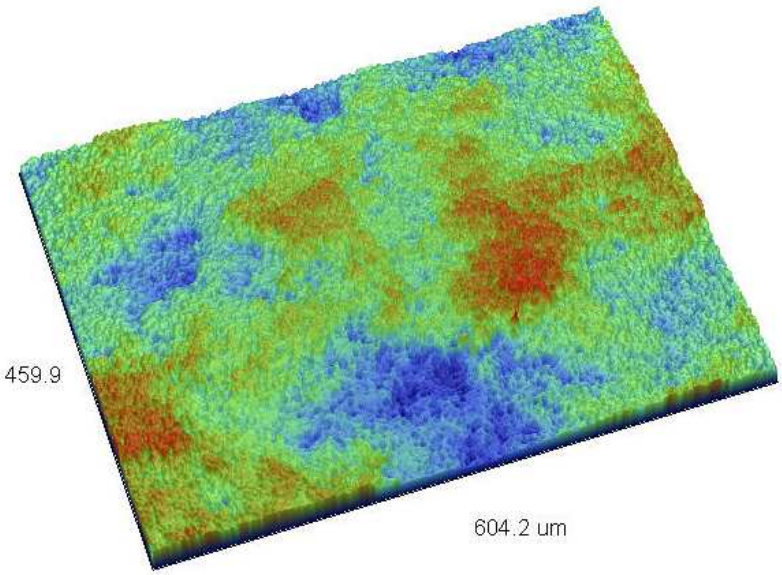

Fig. 6 Profile measurement for portion of vane surface.

Local vane surface temperatures were measured using a Raytec MID10LT^{TM} thermal sensor mounted in a probe holder. This sensor is uncooled. Figure 5 illustrates the probe arrangement, and shows the sensor inclined at an angle of 35°. While the probe diameter at the sensor head is larger than a typical three or five hole pressure probe, being above the measuring plane minimized the flow disturbance in the measuring plane. Surface temperatures were measured by traversing the probe in two of the four slots shown in figure 1. The upstream slot closest to the vane,$(x/C_X = -0.92)$, and the downstream slot farthest from the vane, $(x/C_X = 0.165)$, were used.

Since the IR probe was rotated as well as traversed in the pitchwise direction, several data points were obtained for each streamwise vane location. Each data point had a different spot size. In the plane normal to the probe direction the spot sizes were elliptical. Because of the probe inclination, the major axis was in the spanwise direction. Because of spanwise uniformity, only the width of the minor axis was significant. The probe had a nominal 1:10 spot diameter-to-distance ratio. When the probe axis was normal to the vane surface, and the probe was 2cm from the surface, the spot width was 2.5mm. At 5cm the spot width was 5.5mm. When the surface orientation was 45° to the probe axis the spot size increased by a factor of 1.4.

Roughness measurements. Three dimensional roughness profiles were obtained using a Veeco Instruments WYCO NT1000^{TM} profilometer. Figure 6 shows a typical three-dimensional trace. In this figure the maximum peak-to-valley height was $104\mu m$. Peaks occur in the lower left hand corner, and near the center of the trace. The high center region extends for nearly $200\mu m$ in each direction. The R_a values were between 10 and $14\mu m$ for four samples. The RMS roughness varied between 13 and $18\mu m$, while the maximum peak-to-valley height in each sample was between 96 and $130\mu m$. Additionally, linear roughness traces were made, which showed similar values for R_a.

While the tests were conducted using a sprayed TBC coating, the results are applicable where the roughness is caused by deposition. Jensen et al.[29] in a discussion of surface roughness gave ranges for the roughness height of surface deposits. They showed a range of R_a values between 17 and $32\mu m$, which is close to the values of the TBC roughness used in the work herein. They reported a range of maximum peak-to-valley height from different sources as between 220 and $394\mu m$, which is somewhat greater than the values near $100\mu m$ for the TBC coating.

Using the Koch and Smith[14] approach to determining k_S from the R_a values gives k_S values between 62 and $87\mu m$. A value of $87\mu m$ for k_S corresponds to a value of k_S/C_X of 17×10^{-4}. If normalized by true chord, the value would be reduced by half.

Determination of heat transfer coefficients. The local heat transfer is calculated from the temperature drop across the TBC coating to give the heat flux, and the temperature difference between the surface temperature and the adiabatic recovery temperature. Heat can be transferred by both radiation and convection. The component due to convection is used to calculate the heat transfer coefficient.

$$q_{TOTAL} = k_{TBC}/t_{TBC}(T_{CU} - T_S)$$

$$= q_{CONV} + q_{RAD}$$

Since the measured value of ϵ_S is close to one, and the surroundings also have a high emissivity, q_{RAD} can be approximated by:

$$q_{RAD} = \sigma\epsilon_S(T_S^4 - T_G^4)$$

The gas total temperature, T_G is used rather than the recovery temperature, T_R because, the surroundings were expected to be closer to T_G than to T_R. It will be shown that the radiation heat flux was generally small compared to the convective heat flux.

$$q_{CONV} = h(T_S - T_R)$$

The adiabatic recovery temperature, T_R was calculated from the measured inlet gas total temperature, T_G, and the predicted pressure distribution, using the isentropic relationships and a recovery factor of 0.896. As figure 3 showed, the predicted pressure distributions were in good agreement with the measured pressure distributions.

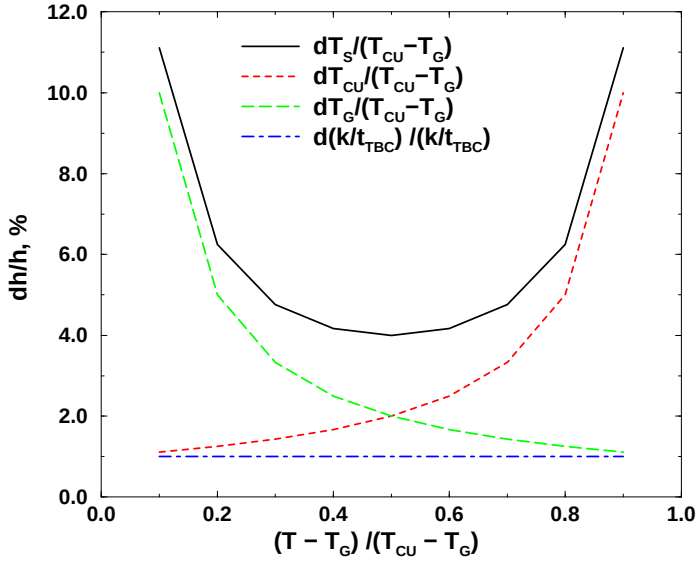

Fig. 7 Variation in h with measured parameters.

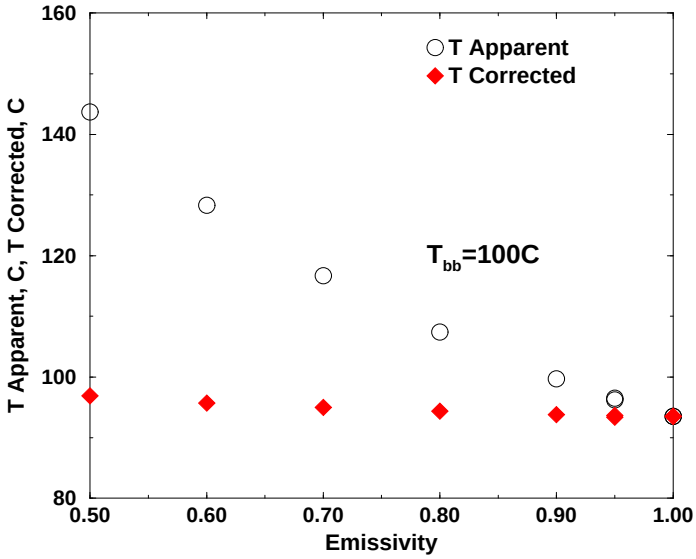

Fig. 8 Corrected temperature versus emissivity settings.

Uncertainty analysis. Figure 7 shows the contribution of the various uncertainties to the overall heat transfer uncertainty. The abscissa is the surface-to-gas temperature difference normalized by the copper-to-gas temperature difference. The ordinate is the percentage uncertainty in h for a one percent uncertainty in the various parameters. The approximately three percent uncertainty in $k_{\rm TBC}/t_{\rm TBC}$ results in the same percentage uncertainty in h or Nu. However, a one percent uncertainty in the normalized value for $T_{\rm S}$ results in a minimum uncertainty of four percent. Doubling the temperature difference, $T_{\rm CU} - T_{\rm R}$, halves the uncertainty in h due to an uncertainty in non-normalized value of $T_{\rm S}$. The minimum uncertainty occurs when $T_{\rm CU} - T_{\rm S} = T_{\rm S} - T_{\rm R}$. At smaller or larger temperature differences, the sensitivity to an uncertainty in $T_{\rm S}$ is even greater. At low heat transfer coefficients the sensitivity of h to $T_{\rm CU}$ is large. But, the sensitivity rapidly decreases as the difference between $T_{\rm CU}$ and $T_{\rm S}$ increases. For nominal test conditions an abscissa of 0.3 corresponds to $Nu = 2500$. An abscissa of 0.5 corresponds to $Nu = 1060$, while an abscissa of 0.8 corresponds to $Nu = 265$.

To minimize the uncertainty in h, several approaches were used to accurately measure $T_{\rm S}$. The primary calibration of the probe sensor was done by comparing the sensor's output with that of a black body thermal source. This was done for temperatures between ambient and 100C. Additional verification was done by viewing the heated vane using both the probe sensor and an infrared camera. There was good agreement between the calibrated sensor's output and the infrared camera's reading when both devices had the same emissivity setting. Imposing a temperature difference of 5C between the sensor head and the probe electronics, did not cause a significant indicated temperature change for the viewed object. This was done because the test section inlet air total temperature was often as much as 5C different from the ambient air temperature.

Since the probe viewed objects at different temperatures and emissivities during the tests, the response of the probe to varying emissivities was needed. The Raytec$^{\rm TM}$ sensor's electronic signal processor has an adjustable emissivity setting. Figure 8 shows the response of a probe to various emissivity settings when viewing a black body source at 100C. This particular sensor reads lower than the black body by 7C when the black body is at 100C and the emissivity setting is 1. As the sensor emissivity setting is decreased, the apparent temperature increases. Figure 8 also shows a corrected black body temperature using the apparent temperature and the emissivity setting. The corrected temperature was obtained assuming that the net energy to the sensor was independent of the emissivity setting. The resulting equation is:

$$T_{\rm CORR} = \left(\epsilon_{\rm S} T_{\rm APP}^4 + (1.0 - \epsilon_{\rm S}) T_{\rm AMB}^4\right)^{0.25}$$

As figure 8 shows, the corrected temperature is almost completely independent of emissivity for a wide range of emissivities.

To determine the surface temperature, the surface emissivity must be known. Figure 9 shows measured emissivity of a TBC sample as a function of wavelength. The IR probe is sensitive in the 8 to 14 micron range. Integrating the measured emissivity over this wavelength range gives an average value of 0.957. Even though the test surface temperatures are only between 20 and 100C, the variation in the temperature weighted emissivity between these two temperatures is small. At a temperature of 20C the calculated emissivity was 0.978, and at 100C the calculated emissivity was 0.983. For the IR detector to measure the correct temperature using an emissivity of 0.98, the detector had to respond uniformly over all wavelengths

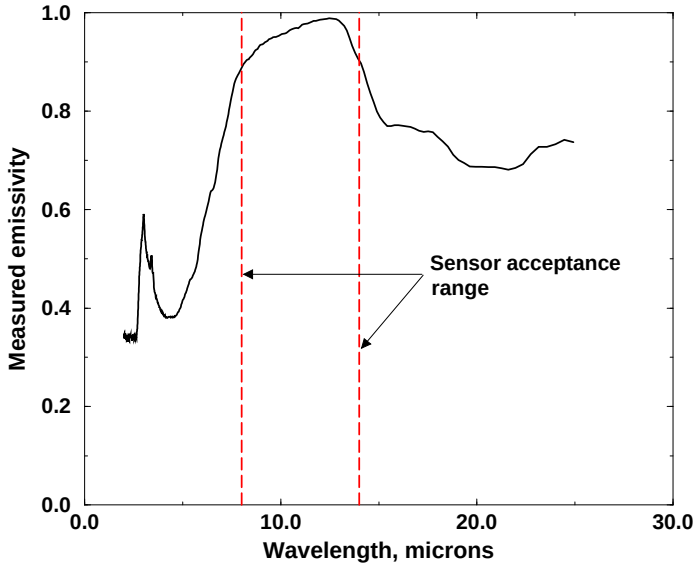

Fig. 9 Measured emissivity.

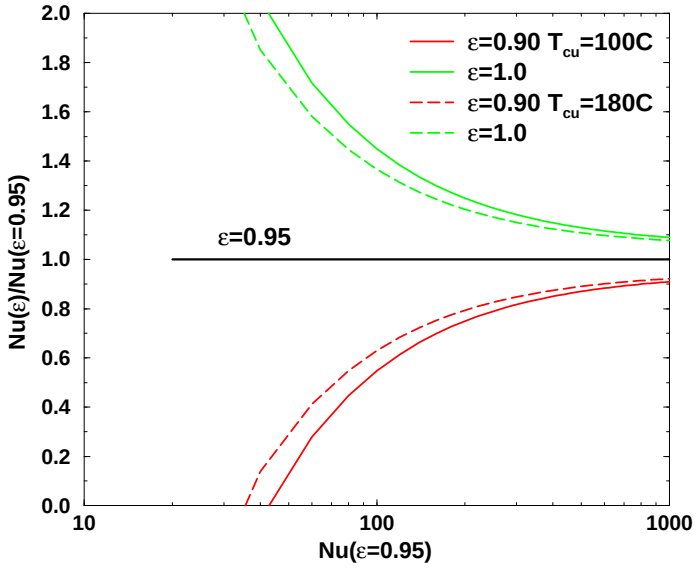

Fig. 10 Effect of emissivity variation on Nusselt number.

between 8 and 14 microns. Since there is a difference between the wavelength averaged emissivity of 0.957 and the energy weighted emissivity of 0.98, the sensitivity of the heat transfer coefficients to emissivity uncertainties was calculated.

Figure 10 illustrates the ratio of Nusselt numbers as a function of predicted Nusselt numbers for surface emissivity variations of ±0.05. The variations are very large. These curves are primarily for illustration, since the expected uncertainty in surface emissivity is about ±0.01. When the assumed emissivity is 0.95, and the actual emissivity is 0.90, the actual heat transfer is zero at a predicted Nusselt number of 42. While the IR detector indicates a

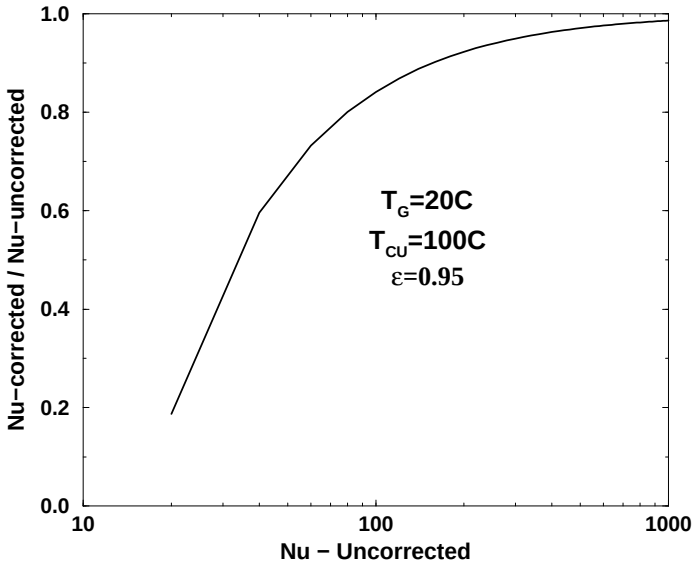

Fig. 11 Effect of radiation correction on heat transfer.

small temperature drop across the TBC coating, in actuality there is none. Only at very high Nusselt numbers is the sensitivity to uncertainties in the surface emissivity small. The other item of note in this figure is that doubling the gas-to-vane temperature difference results in only a small reduction in the sensitivity to surface emissivity. This is in contrast to uncertainties associated with temperatures. Figure 7 shows that doubling the vane to surface temperature difference halves the uncertainty in heat transfer coefficient.

The surface temperatures used in this experiment are greater than are typically seen in liquid crystal experiments. Figure 11 illustrates that the radiation correction can be significant at low Nusselt numbers. The radiation correction was applied for all data points. At low Nusselt numbers the temperature difference across the TBC insulating layer is small, and figure 7 shows that temperature uncertainties can be larger than the radiation correction.

DISCUSSION of RESULTS

The previous discussion showed that the measurements can have significant uncertainty, especially at low Reynolds numbers. However, there is no reason to believe that a bias has been introduced into the measurements. Vane leading edge region heat transfer data is compared with experimentally derived correlations in order to validate the present experimental measurements. The vane Nusselt numbers in the leading edge region are in the midrange of Nusselt numbers. The data of Stripf et al.[1] showed that increasing surface roughness at constant Reynolds number served to bring the suction surface transition location forward.

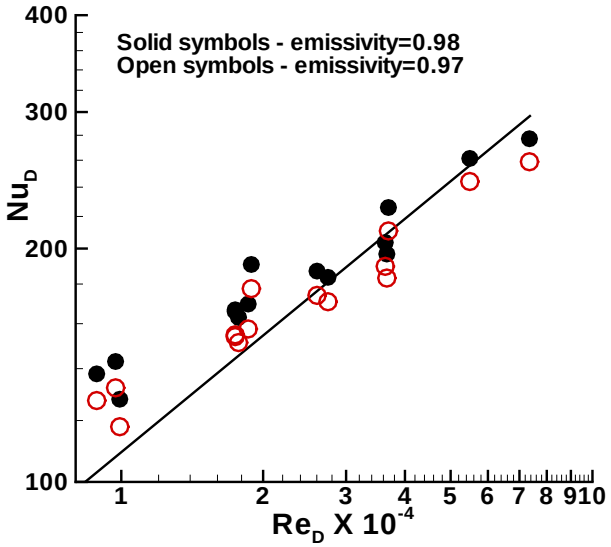

Fig. 12 Leading edge heat transfer comparisons.

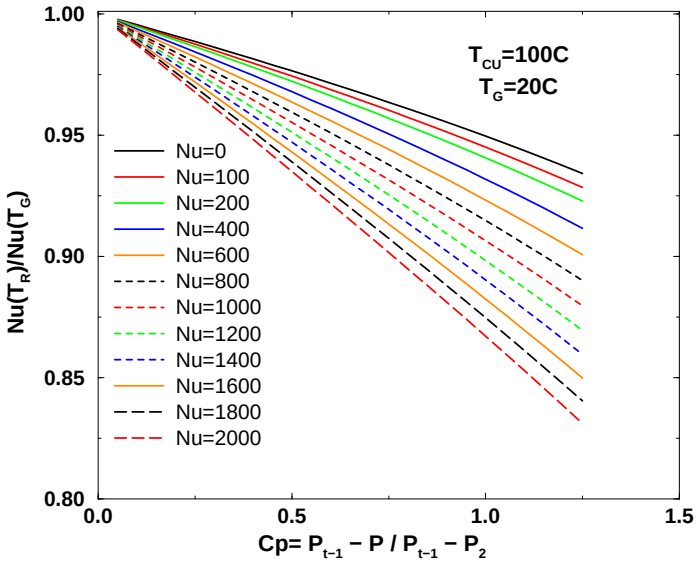

Fig. 13 Effect of recovery factor on Nusselt number.

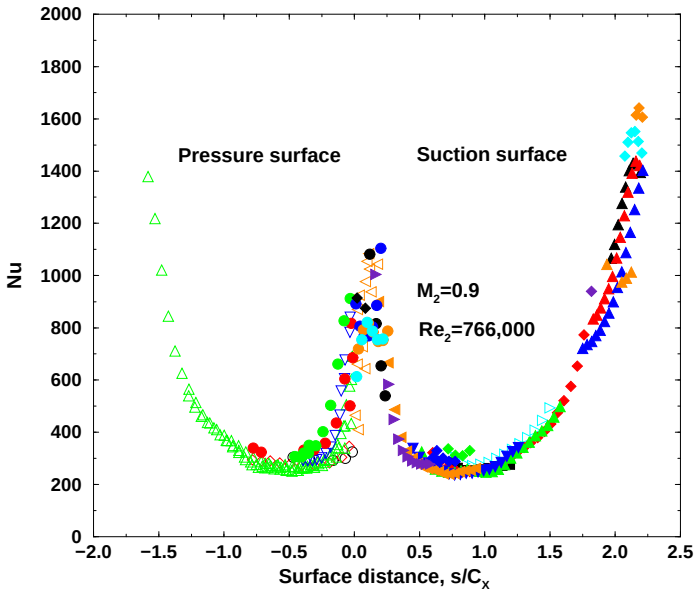

Fig. 14 Sample data at one flow condition.

Until transition due to roughness reaches the leading edge, there was only a slight increase in leading edge heat transfer for an inlet true chord Reynolds number,$(Re(C))$ of 1.4×10^5 or lower. When the Reynolds number was increased to 2.5×10^5 there was an increase in leading edge heat transfer of nearly 20%, over the smooth surface value for the largest roughness height. This height was $k/C = 8.5 \times 10^{-4}$. This value corresponded to $k_S/C = 18.8 \times 10^{-4}$, using the Waigh and Kind[18] correlation. The Koch and Smith[14] correlation gave $k_S/C = 8.4 \times 10^{-4}$. The maximum inlet Reynolds number for the results herein is nearly twice the maximum value of Stripf et al.[1]. The Koch and Smith[14] value for k_S/C nearly equals their maximum value. It is expected, therefore, that for our work the leading edge will not be affected by roughness for other than the highest inlet Reynolds numbers.

Sanitjai and Goldstein[30] give a correlation for the leading edge heat transfer for cylinders in crossflow at low turbulence intensities. The form of the correlation is:

$$Nu_D = C_{SG} Re_D^{0.5} Pr^{0.35}$$

The constant, C_{SG} equals 1.11 at the stagnation point, and 0.945 for the average heat transfer between 0 and 85° from the stagnation point. The spot size is not infinitesimal. When the probe is directly in front of the vane, the included angle of the spot is less than 20°. The stagnation point value for C_{SG} is more appropriate for comparison purposes. Figure 12 shows the experimental leading edge Nusselt numbers, and a line corresponding to the correlations of Sanitjai and Goldstein[30] for the stagnation region. The abscissa is the effective Reynolds number, which accounts for leading edge blockage. At higher Reynolds numbers the measurements agree well with the correlation. At lower Reynolds numbers, with their correspondingly low Nusselt numbers, the data are significantly higher than the correlation. Since the heat transfer is much more sensitive to measurement uncertainty at low Nusselt numbers, this is not surprising. On the other hand, Hoffs et al.[20] showed that the Frossling number, $Nu_D/Re_D^{0.5}$, decreased by about 10% as Re_D decreased from 109,000 to 25,000 at low turbulence. They point out that their results are consistent with the correlation of Dullenkopf and Mayle[31]. The leading edge diameter-to-axial chord ratio is 0.286, giving $Nu = 3.5 Nu_D$. The implication of figure 12 that vane chord Nusselt numbers may be over estimated

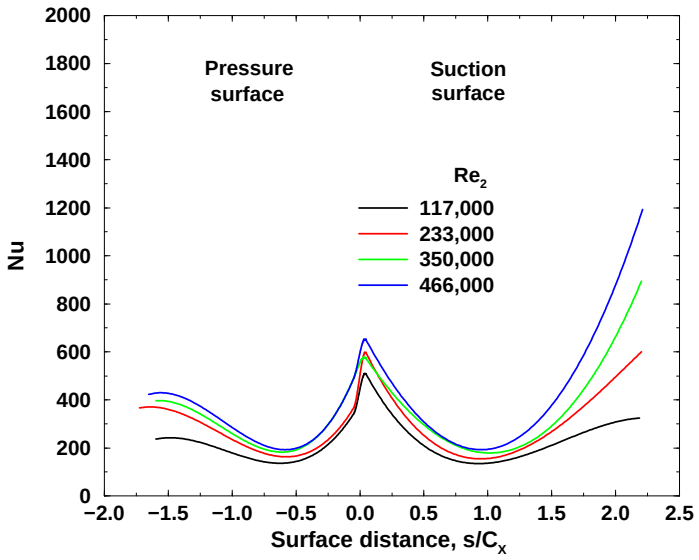

Fig. 15a Experimental heat transfer for $M_2 = 0.3$.

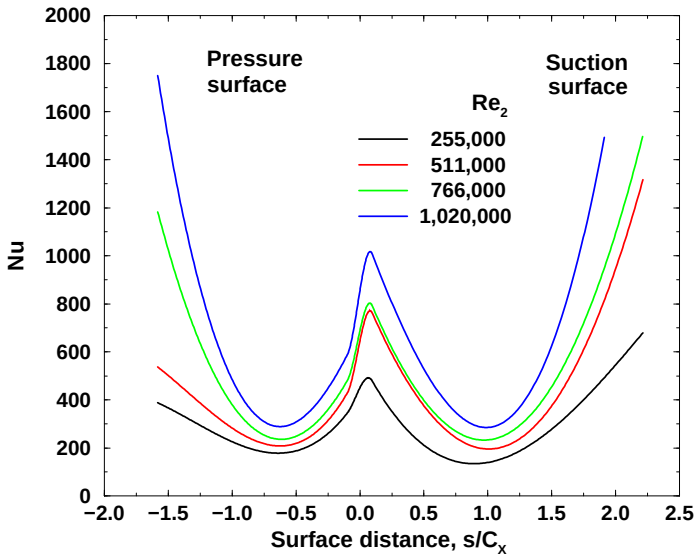

Fig. 15b Experimental heat transfer for $M_2 = 0.9$.

by more than 20% for $Nu < 350$ is mitigated by the data of Hoffs et al.[20], which imply that the overestimation is only about 10%. As Nu increases the overestimation is less. Fortunately, roughness effects are likely to be seen at much higher Nusselt numbers. A fit to the experimental data yields an exponent of 0.34, which is consistent with the data of Hoffs et al.[20], but less than the 0.5 value of the correlation.

Figure 12 also shows open symbols, where the experimental data were recalculated using an emissivity of 0.97. This shows high Nusselt number sensitivity to emissivity. At low Reynolds numbers the recalculated data agree better with the correlation. Accounting for the results of Hoffs et al.[20], gives no overestimation at an emissivity of 0.97.

Heat transfer coefficients should be based on T_{R}, but are sometimes calculated using T_{G}. Figure 13 shows that using recovery instead of total temperature reduces Nu by nearly 15% at $C_p = 1.25$, when $M_2 = 0.9$ and $Nu(T_{\mathrm{G}}) = 2000$. Ratios are nearly linear in C_p. Reducing M_2 to 0.3 is equivalent to reducing C_p by a factor of 6.7.

Figure 14 shows data for the case of $M_2 = 0.9$ and $Re_2 = 766,000$. Data were taken at different pitchwise locations and different probe angles, and for traverses in front of and behind the vane. Data are shown for both test vanes, and there is considerable overlap in the leading edge region. Several symbols are shown on the figure. Each test vane or traverse has a unique data symbol. The same symbol was sometimes used for more than one probe angle. Not all data that were recorded are shown. If the sensor saw both the background and the vane, the recorded temperature was less than the true vane temperature. These readings gave higher than actual Nusselt numbers, and could be confidently eliminated because lower and consistent Nusselt numbers were calculated from other probe positions viewing the same vane surface location.

Although not shown, tests with $T_{\mathrm{CU}} - T_{\mathrm{G}}$ approximately halved gave very similar Nu distributions. This indicates that, while the sensitivity to temperature uncertainties may be high, the actual temperature errors are not large.

For each flow condition there are several hundred data readings. There is also a very small, but unavoidable, variation in the spot location between different flow conditions. In addition to slight angular and position variations, the aerodynamic forces on the probe vary with dynamic pressure. For the purpose of clarity, curve fits were used to present the data results. Nusselt numbers at different Reynolds numbers can be relatively close. When the flow is laminar, a 30% increase in Reynolds number yields less than a 15% increase in Nusselt number.

Figures 15a and 15b show data for all Reynolds numbers at $M_2 = 0.3$ and $M_2 = 0.9$. The pressure surface data for the four Reynolds numbers at the lower Mach number do not indicate a strong roughness effect. In contrast, the pressure surface data at the two higher Reynolds numbers at $M_2 = 0.9$ indicate a strong roughness effect. In figure 15b very high heat transfer rates are seen for the last 40% of the pressure surface. At similar Reynolds numbers the shape of the pressure surface heat transfer distributions are different between the two Mach numbers. Figure 3 shows that the favorable pressure gradient starts earlier at the lower Mach number. This is the likely cause of the different pressure surface heat transfer distributions. In an overall sense, similar Reynolds numbers give similar heat transfer rates for both Mach numbers. For the rear of the pressure surface, Stripf et al.[1] showed only small increases in heat transfer for all but their highest roughness. However, for that roughness the increase in heat transfer was up to a 400% greater than the smooth vane, when the inlet Reynolds number was also at a maximum.

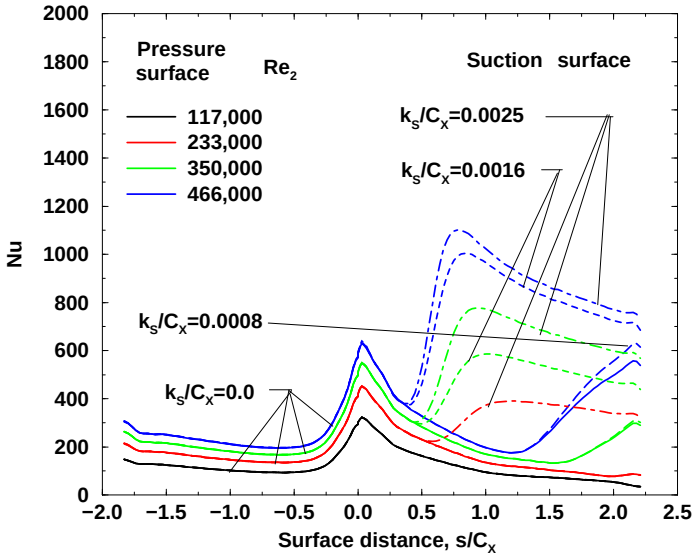

Fig. 16a Predicted heat transfer for $M_2 = 0.3$.

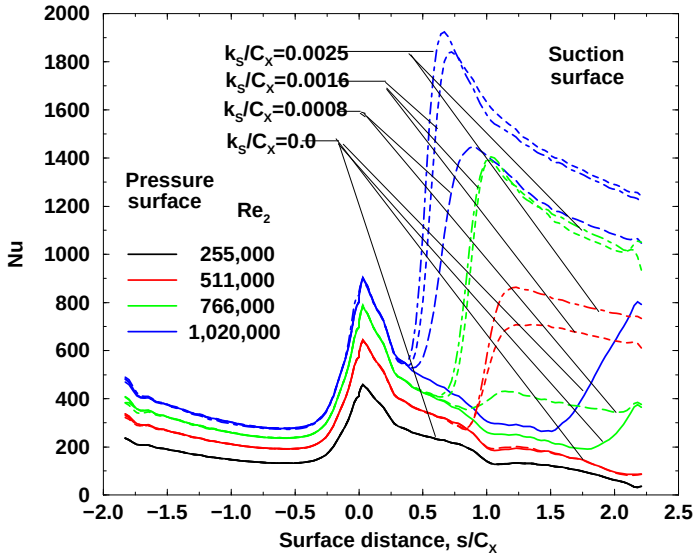

Fig. 16b Predicted heat transfer for $M_2 = 0.9$.

The consequences of the inevitable data scatter are seen on the forward part of both the pressure and suction surfaces. Figure 15b shows that increasing the Reynolds number by a factor of four causes the leading edge heat transfer to, as expected, double. Figure 15a shows that at the lower Mach number the ratio in Nusselt numbers is less. This is most likely do to a combination of higher uncertainties and a reduced Frossling number consistent with the data of Hoffs et al.[20]. Their leading edge data agree with the correlation of Dullenkopf and Mayle[31].

On the rear half of the suction surface heat transfer consistent with transition is seen at all Reynolds numbers, even at $M_2 = 0.3$. Beyond the throat, there is no longer a favorable pressure gradient, and roughness is more likely to cause transition. The rear of the suction surface sees very high Nusselt numbers. Even for smooth vanes, very high heat transfer rates near the rear of the suction surface have been reported at low turbulence intensities. For example, the data of Arts et al.[32] show this behavior.

Neither the raw data nor curve fits show a rapid increase in suction surface heat transfer consistent with abrupt transition. This could partially be due to the relatively large spot size near the throat. The spot size approaches $0.4C_X$ in this region. Even though figure 14 shows the spots closely spaced, there is a great deal of overlap between adjacent spots in a traverse. On the other hand, a long transition length for a rough surface is consistent with the data of Gibbings and Al-Shukri[33]. Their data showed that at a turbulence intensity of 0.9% the transition length for a rough surface is nearly four times longer that the transition length at a turbulence intensity of 4.6%. Even though their data is at turbulence intensities of 4 and 8&, Stripf et al.[1] show transition lengths varying from very abrupt to being an axial chord long. Lateral conduction within the relatively thick TBC layer is not expected to have smoothed out the Conduction heat transfer.

calculations done with an abrupt external heat transfer distribution did not show a significant smoothing out of the heat transfer.

Figures 15a and b show that, for similar Reynolds numbers, the Mach number effect on heat transfer is not large for the rear of the suction surface. For these measurements the probe was behind the vane. For the same Reynolds number the aerodynamic loads on the probe at $M_2 = 0.9$ are about three times greater than at $M_2 = 0.3$. The distortion of the spot location due to aerodynamic loads does not appear to have been significant.

Computational results. Predictions for vane rough surface heat transfer were in the main unsucessfull. Figure 16 shows the predictions. Roughness effects were incorporated using the algebraic roughness model of Cebeci and Chang[34]. The code successfully predicted smooth surface heat transfer under a variety of flow conditions, (Boyle and Simon[35]). Since the tests herein were at low turbulence intensity, the rapid increase in suction surface heat transfer is the result of a roughness transition model. This model was described by Boyle and Senyitko[25]. Clearly, this model is at the heart of the disagreement between measured and predicted suction surface heat transfer. The short transition length in the model is not evidenced in the data. Calculations are shown for different roughness heights. No pressure surface transition was predicted. But, the high Reynolds number data clearly show increased heat transfer, consistent with transition.

At both exit Mach numbers predictions show smooth surface, $k_S/C_X = 0$, suction surface transition for the two highest Reynolds numbers. Even though the highest Reynolds number at $M_2 = 0.3$ is about the same as the second lowest Reynolds number at $M_2 = 0.9$, the C_p distributions are different. The differences in the C_p distributions are the cause of the differences in transition behavior at the same Reynolds number.

Calculations are shown for k_S/C_X values of $0,8 \times 10^{-4}, 16 \times 10^{-4}$, and 25×10^{-4}. Using the R_a measurements, the Koch and Smith[14] correlation gives k_S/C_X between 12 and 17 $\times 10^{-4}$. The Koch and Smith correlation is relatively easy to calculate. More importantly, the sequence in which different roughness geometries departed the smooth suction surface heat transfer curve in the data of Stripf et al.[1] was better predicted using the Koch and Smith[14] correlation, than by using the Waigh and Kind[18] correlation.

At high Reynolds numbers calculations show only a very small heat transfer increase between the two largest roughness heights. In the Cebeci-Chang[34] roughness model the increase in mixing length due to roughness reaches an asymptotic value which depends only on flow conditions.

Very rapid roughness transition is predicted, even though a roughness transition length model is used. The data show a much longer transition length. The suction surface heat transfer near the trailing edge is in reasonable agreement with the data. This indicates that the cause of the disagreement is not the roughness turbulence model. The poor agreement before the trailing edge indicates that the roughness transition model is in error.

After transition the predictions show a strong dependency on the equivalent roughness height. Near the trailing edge the results are in contrast with those of Stripf et al.[1]. In their work all suction surface heat transfer distributions return to the smooth surface values just prior to the trailing edge. The figure 16 shows increased in heat transfer with roughness all the way to the trailing edge.

Roughness models, whether they be algebraic or two equation, (eg. Wilcox[36], Aupoix and Spalart[37]) depend on knowing the equivalent roughness height. The equivalent roughness height is determined from roughness measurements using correlations. As mentioned earlier, several correlations for determining the equivalent roughness height have been developed. The choice of which correlation is appropriate is still somewhat problematic. Stripf et al.[1] tested vanes with deterministic roughness, and calculated equivalent roughness heights using the correlation of Waigh and Kind[18]. The tests showed a strong influence of surface roughness on vane suction side heat transfer. However, the Waigh and Kind[18] correlation did not accurately predict the increase in heat transfer. Higher equivalent heights did not consistently result in either earlier transition, or higher heat transfer rates.

CONCLUDING REMARKS

This work showed that probe mounted thermal detectors can be used to map vane surface temperatures in a cascade environment. Accurate surface temperatures using infrared measurements were highly dependent on knowledge of surface emissivity. In this experiment the accuracy of lower Nusselt numbers were sensitive to accurate surface temperatures. Comparisons with the data of others showed that the heat transfer measurements were reasonably accurate, and consistent with other experimental results.

These experiments were conducted at a turbulence intensity of 1%. The vane heat transfer distributions were different in shape from those measured be others at a higher inlet turbulence intensity. This illustrates the desirability of measuring rough surface heat transfer with turbulence levels and scale consistent with engine conditions.

A reduced spot size-to-chord ratio would be helpful. Besides increasing the chord, narrowing the field of view, or reducing the probe diameter would be useful. A reduced probe diameter would allow the probe to get closer to the blade surface, and would lessen the twisting forces on the probe. The latter being important in high speed flows.

Heat transfer rates in the leading edge region, and for the first quarter of both the suction and pressure surfaces were consistent with predictions for smooth surface laminar heat transfer. Because of the low turbulence intensity, predictions for a smooth pressure surface gave laminar heat transfer over the entire range of Reynolds numbers. In these predictions the heat transfer level is approximately constant over the rear half of the pressure surface. The data, however showed increasing heat transfer in this region. At the lower Reynolds numbers the pressure surface heat transfer leveled off near 80% of the pressure surface distance. At higher Reynolds numbers the pressure surface Nusselt numbers increased continuously to the pressure surface trailing edge.

Because predictions are sensitive to k_S, accurate means of determining k_S from roughness measurements need to be verified.

Heat transfer on the rear portion of the suction surface was similar to that on the rear of the pressure surface. In all cases heat transfer rates increased from a minimum value near midway on the suction surface. No plateau was seen in the suction surface heat transfer rates, even at the lowest Reynolds numbers. Very high heat transfer rates were seen near the rear of the suction surface. At the highest Reynolds numbers, the experimental heat transfer rates near the rear of the suction surface were nearly twice the leading edge rates.

REFERENCES

1. Stripf, M., Schultz, A., and Wittig, S., 2004, "Surface Roughness Effects on External Heat Transfer of a HP Turbine Vane," ASME paper GT2004-53114.

2. Barlow, D.N., Kim, Y.W., and Florschuetz, L.W., 1997, "Transient Liquid Crystal Technique for Convective Heat Transfer on Rough Surfaces," ASME *Journal of Turbomachinery,* Vol. 119, pp. 12-22.
3. Hosni, M.H., Coleman, H.W., Taylor, R.P., 1998, "Rough-Wall Heat Transfer in Turbulent Boundary Layers," *Int. Journal of Fluid Mechanics Research* Vol. 25, pp. 212-219
4. Bogard, D.G., Schmidt, D.L., and Tabbita, M., 1998, "Characterization and Laboratory Simulation of Turbine Airfoil Surface Roughness and Associated Heat Transfer," ASME *Journal of Turbomachinery,* Vol. 120, pp. 337-342.
5. Blair, M.F., 1994, "An Experimental Study of Heat Transfer in a Large Scale Turbine Rotor Passage," ASME *Journal of Turbomachinery,* Vol. 116, pp. 1-13.
6. Bons, J.P., 2002, "St and Cf Augmentation for Real Turbine Roughness with Elevated Freestream Turbulence,", ASME paper GT-2002-30198.
7. Bons, J.P., and McClain, S.T., 2003, "The Effects of Real Turbine Roughness with Pressure Gradient on Heat Transfer," ASME paper GT-2003-38738.
8. Boyle, R.J., Spuckler, C.M., Lucci, B.L., and Camperchioli, W.P, 2001, "Infrared Low-Temperature Turbine Vane Rough Surface Heat Transfer Measurements," ASME *Journal of Turbomachinery,* Vol. 123, pp. 168-177.
9. Abuaf, N., Bunker, R.S., Lee, C.P., 1998, "Effects of Surface Roughness on Heat Transfer and Aerodynamic Performance of Turbine Airfoils," ASME *Journal of Turbomachinery,* Vol. 120, pp. 168-177.
10. Bunker, R.S., 1997, "Separate and Combined Effects of Surface Roughness and Turbulence Intensity on Vane Heat Transfer," ASME paper 97-GT-10.
11. Tarada, F., and Suzuki, M., 1993, "External Heat Transfer Enhancement to Turbine Blading Due to Surface Roughness, ASME paper 93-GT-74.
12. Taylor, R.P., 1990, "Surface Roughness Measurements on Gas Turbine Blades," ASME *Journal of Turbomachinery,* Vol. 112, pp. 175-180.
13. Bons, J.P., Taylor, R.P., McClain, S.T., and River, R.B., 2001, "The Many Faces of Surface Roughness," ASME paper 2001-GT-163.
14. Koch, C.C., and Smith, L.H., 1976, "Loss Sources and Magnitudes in Axial-Flow Compressors," ASME *Journal of Engineering for Power* Vol. 98, pp. 411-424.
15. Sigal, A. and Danberg, J. E., 1990 "New Correlation for Roughness Density Effect on Turbulent Boundary Layers," AIAA *Journal* Vol. 28 pp. 554-556.
16. Dvorak, F.A., 1969, "Calculation of Turbulent Boundary Layers on Rough Surfaces in Pressure Gradient," AIAA *Journal* Vol. 7 pp. 1752-1759.
17. Dirling, R.B., 1973, "A Method for Computing Rough-wall Heat Transfer Rates on Re-Entry Nosetips," AIAA paper 73-763.
18. Waigh, D.R. and Kind, R.J., 1998, "Improved Aerodynamic Characterization of Regular Three-Dimensional Roughness," AIAA *Journal* Vol. 36 pp. 1117-1119.
19. van Rij, J.A., Belnap, B.J., and Ligrani, P.M., 2002, "Analysis and Experiments on Three-Dimensional Irregular Surface Roughness," ASME *Journal of Fluids Engineering,* Vol. 124, pp. 671-677.
20. Hoffs, A., Drost, U., and Bolcs, A., 1996, "Heat Transfer Measurements on a Turbine Airfoil at Various Reynolds Numbers and Turbulence Intensities Including Effects of Surface Roughness," ASME paper 96-GT-169.
21. Sargent, S.R., Hedlund, C.R., and Ligrani, P.M., 1998, "An Infrared Thermography Imaging System for Convective Heat Transfer Measurements in Complex Flows," Meas. Sci. Technol., Vol. 9, pp. 1974-1981.
22. Balduf, S., Schultz, A., and Wittig, S., 1999, "High Resolution Measurements of Local Heat Transfer Coefficients by Discrete Hole Film Cooling," ASME paper 99-GT-43.
23. Johnson, C.A., Bogard, D.G., and McWaters, M.A., 1999, "Highly Turbulent Effects on Film Cooling of a Simulated Airfoil Leading Edge," ASME paper 99-GT-261.
24. Sweeney, P.C., and Rhodes, J.F., 2000, "An Infrared Technique for Evaluating Turbine Airfoil Cooling Designs," ASME *Journal of Turbomachinery,* Vol. 122, pp. 171-178.
25. Boyle, R.J., and Senyitko, R.G.,2003, "Measurements and Predictions of Surface Roughness Effects on Turbine Vane Aerodynamics," ASME paper GT-2003-38580.
26. Schwab, J.R., 1982, "Aerodynamic Performance of High Turning Core Turbine Vanes in a Two-Dimensional Cascade," NASA TM 82894. 27. Chima, R.V., 1987, "Explicit Multigrid Algorithm for Quasi-Three-Dimensional Flows in Turbomachinery," AIAA *Journal of Propulsion and Power,* Vol. 3, pp. 397-405.
28. Chima, R.V., Giel, P.W., Boyle, R.J., 1993, "An Algebraic Turbulence Model for Three-Dimensional Viscous Flows," AIAA paper 93-0083, (NASA TM-105931).
29. Jensen, J.W., Squire, S.W., Bons, J.P., and Fletcher, T.H,, 2004, "Simulated Land-Based Turbine Deposits Generated in an Accelerated Deposition Facility," ASME paper GT2004-53324.
30. Sanitjai, S., and Goldstein, R.J., 2004, "Forced Convection Heat Transfer From a Circular Cylinder in Crossflow to Air and Liquids." *Int. Journal of Heat and Mass Transfer,*, Vol. 47, pp. 4795-4805.
31. Dullenkopf, K., Mayle, R.E., 1995, "An Account of Free-Stream Turbulence Length Scale on Laminar Heat Transfer," ASME *Journal of Turbomachinery,* Vol. 117, pp. 432-439.
32 Arts, T., Lambert de Rouvroit, M., and Rutherford, A.W., 1990, "Aero-Thermal Investigation of a Highly Loaded Transonic Linear Turbine Guide Vane Cascade," VKI Technical Note 174.
33. Gibbings, J.C., and Al-Shukri, S.M., 1997, "Effect of Sandpaper Roughness and Stream Turbulence on the Laminar Layer and its Transition," *The Aeronautical Journal,* Vol. 101, pp. 17-24.
34. Cebeci, T., and Chang, K.C., 1978, "Calculations of Incompressible Rough-Wall Boundary Layer Flows," AIAA *Journal,* Vol. 16, pp. 730-735.
Boyle, R.J., and Simon, F.F., 1999, "Mach Number Effects on Turbine Blade Transition Length Predictions," ASME *Journal of Turbomachinery,* Vol. 121, pp. 694-702.
36. Wilcox, D.C., 1994, "*Turbulence Modeling for CFD,* DCW Industries, Inc. La Canada, CA
37. Aupoix, B., and Spalart, P.R., 2003, "Extension of the Spalart-Allmaras Turbulence Model to Account for Wall Roughness," *Int. Journal of Heat and Fluid Flow,*, Vol. 24, pp. 454-462.